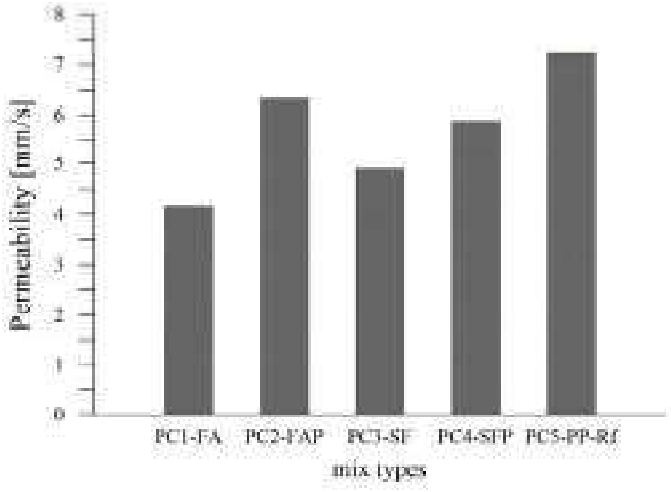


| Mix type | Standard error |
|---|---|
| PC1-FA | 0.11 |
| PC2-FP | 0.34 |
| PC3-SF | 0.31 |
| PC4-SP | 0.32 |
| PC5-PP-Rf | 0.36 |

(**a**)

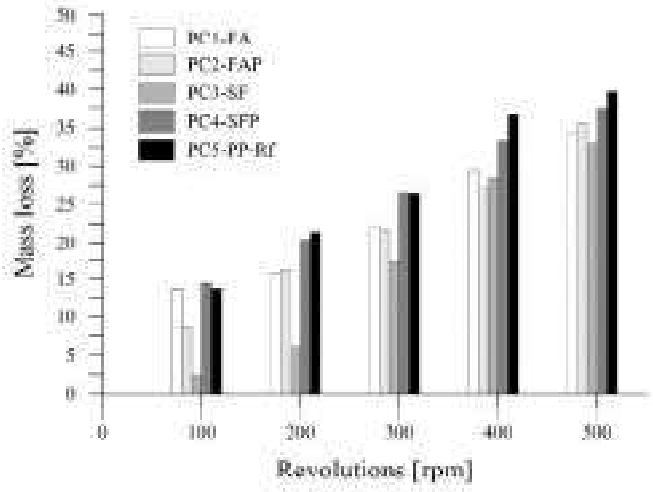


(**b**)

**Figure 8.** Permeability (**a**) and Cantabro mass loss (**b**) after 28 d of curing.

### *3.3. Durability of Pervious Concrete*

The durability of the pervious concrete was assessed based on the raveling and freeze–thaw resistance. The raveling resistance was measured using the Cantabro mass loss test, and the freeze–thaw resistance was determined at (−18 ± 2) °C and (22 ± 2) °C in a freeze–thaw chamber to determine the damage mechanism.

#### 3.3.1. Raveling Resistance

The influence of silica fume, fly ash, and polypropylene fibers on the 28-day raveling resistance is shown in Figure 8b. Mass loss manifests the abrasion quality during the (LA) abrasion test. The incorporation of cementitious materials (such as SF and FA) along with fiber reinforcement provides bridging mechanisms between the components of pervious concrete. Figure 8b shows that the mass loss associated with the deterioration of the specimens increased with an increase in the number of cycles. After 500 cycles, all mixtures exhibited a failure pattern, where coarse aggregates detached from the surface and corner edges, resulting in progressive damage. The PC3-SF mixture exhibited the lowest mass loss (<22%) due to its dense microstructure and improved interlocking strength resulting from the physical filling effect and the pozzolanic reaction of silica fume. The fly ash-based mixture, PC1-FA, showed a more significant mass loss during the test than PC3-SF because of the later strength gain of PC1-FA, owing to the delayed pozzolanic reaction. The use

of PPFs with fly ash (PC2-FAP) and silica fume (PC4-SFP) resulted in a slightly higher final mass loss than the mixture with fly ash (PC1-FA) and silica fume (PC3-SF). This increase in mass loss could be attributed to the higher porosity and permeability of the mixes containing PPFs in this study. For the same reason, the inclusion of PPFs without other admixtures decreased the overall degradation resistance.

#### 3.3.2. Freeze–Thaw Resistance

The impact of silica fume, fly ash, and polypropylene fibers on the 28-day freeze–thaw resistance of pervious concrete is shown in Figure 9. The freeze–thaw resistance can be divided into three stages. During stage I, no noteworthy variation in mass loss was observed (until 100 cycles). In stage I of freeze–thaw cycling, the degree of saturation (DOS) was low, and insignificant deterioration occurred, except for PC2-FAP with a higher DOS. In stage II, the mass loss variation was more evident owing to the raveling or disintegration of aggregates, debonding, and cement paste spalling. The mass loss of the fly ash-based mixture (PC1-FA) and fiber-reinforced fly ash mixture (PC2-FAP) grew much faster and was accelerated by the substantial uptake of water during consecutive freeze–thaw cycles.

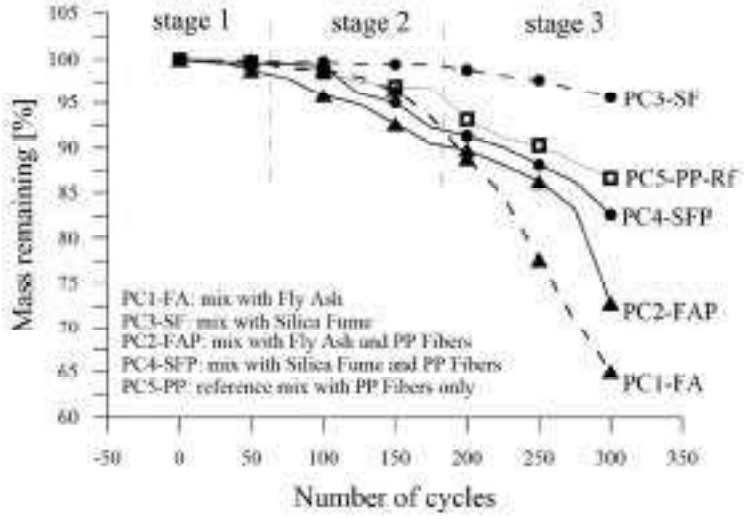


**Figure 9.** Freeze-thaw durability performance based on mass loss criteria.

During stage II, the frost-heaving stress (FHS) builds up with a critical degree of saturation, leading to serious micro-damage development with a progressive increase in freeze–thaw cycling. The FHS depends on the air voids and the degree of saturation of the specimens; therefore, mixtures with more air voids and full saturation exhibited more mass loss and a higher degree of damage evolution (this condition has also been observed in [64]). In stage III, the variation in the mass loss was more abrupt and sharp, indicating serious micro- and macro-damage evolution, with obvious surface cracks developing in the specimens that partially passed through the cement paste, and the aggregate interface further aggravated the debonding of the aggregate with increasing freeze–thaw cycling. A silica fume-based (PC3-SF) mixture with a dense microstructure increased the resistance to frost damage during all three stages of freeze–thaw cycling. The incorporation of fibers in pervious concrete provides a reinforcing effect to bridge the crack propagation and strengthen the bond among concrete components, thus efficiently enhancing the freeze–thaw performance of reinforced (PC5-PP-Rf) pervious concrete. The effectiveness of PPFs in enhancing the freeze–thaw performance of silica fume (PC4-SFP) and fly ash-based (PC2-FAP) reinforced mixes were found to be highly distinct, which was attributed to their unique pore structure characteristics. In stage III, the deterioration rate was drastic because the bridging mechanisms of the fiber were not capable of avoiding the cracks and resisting the expansive stresses built up during the continuous freeze–thaw cycling; thus, a slight improvement in the freeze–thaw performance was achieved.

### *3.4. Hydration Product Analysis of the Cement Past Containing Fly Ash and Silica Fume*

#### 3.4.1. TGA-DTA Measurement

The TGA-DTA curves of cement paste containing fly ash (FPC1) and silica fume (SPC2) are illustrated in Figure 10. Three different major endothermic peaks occurred in the temperature ranges of 100–150 °C, 400–500 °C, and 700–800 °C. The first endothermic peaks found at 100–150 °C were primarily due to the dehydroxylation of the calcium silicate hydrate (C-S-H) phase. The second endothermic peak identified at 400–500 °C is attributed to the dehydration and decomposition of portlandite $Ca(OH)_2$ (this is consistent with [65,66]). The addition of fly ash substantially influences the DTA profile, causing a reduction in the endothermic peaks at higher temperatures. Calcium carbonate decomposition occurs at 700~800 °C. The analysis of TG and DTG results indicates that the addition of fly ash or silica fume enhances the formation of hydration products through a pozzolanic reaction.

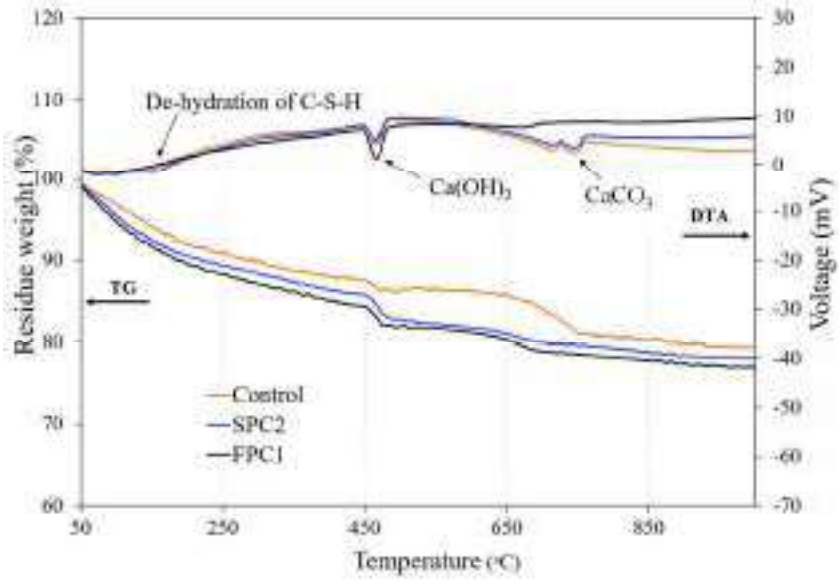


**Figure 10.** TGA-DTA profiles of control and binder cement pastes after 28 days.

#### 3.4.2. XRD Spectra

The XRD diffractograms of the standard and blended cement pastes at 28 days are shown in Figure 11a. The relative peak intensity of $Ca(OH)_2$ in the blended paste (SPC2) was lower than that of the reference paste without silica fume. However, stronger $Ca(OH)_2$ peaks were observed for the fly ash-blended paste (FPC1) because of its slower pozzolanic reactivity. It is reported that the pozzolanic reactivity of fly ash is slower than cement hydration, and the extent of fly ash reaction for blended paste with a water/binder ratio (W/C) equal to 0.5 and an FA content of 25% is approximately 10% to 14% at the age of 28 days. According to Hanehara et al. [67], the extent of fly ash reactivity increased to approximately 25% at the age of 1 year for blended cement paste produced with a W/C ratio of 0.5 and an FA content of 40%. The $CaCO_3$ peaks observed in all pastes could be attributed to natural carbonation. The precipitation of $Ca(OH)_2$ and C-S-H on the etched surface of fly ash particles, with an increase in the pozzolanic reaction, reinforces the contact bonding between fly ash and cement as well as fly ash particles. This would ultimately make the microstructure denser and more homogeneous and result in a remarkable long-term strength gain.

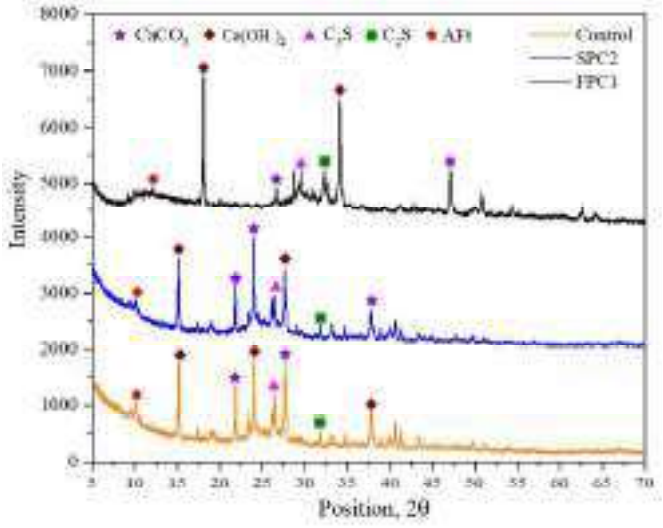


(a)

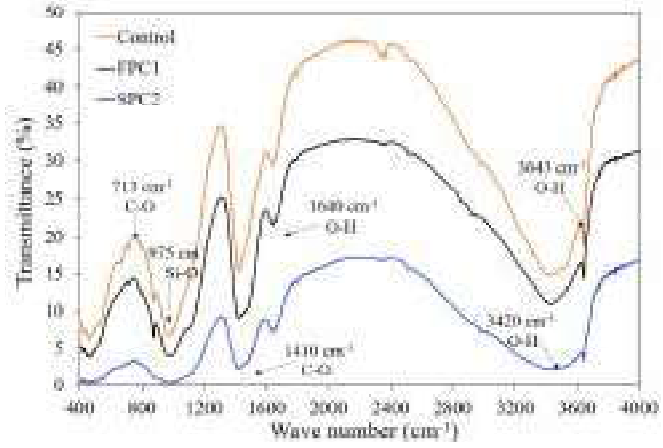


(b)

**Figure 11.** XRD spectrum (**a**) and FTIR spectra (**b**) of control and binder cement paste at 28 days of standard curing.

#### 3.4.3. FTIR Spectra Analysis

FTIR measurements were performed to demonstrate the mineral variations caused by fly ash in FPC1 and silica fume in the SPC2 mix, as shown in Figure 11b. The absorption peaks at 3420 $cm^{-1}$ are attributed to the vibrational bending of O-H groups in water, and the bending at 1640 $cm^{-1}$ is associated with the O-H groups. The other O-H band at 3643 $cm^{-1}$ originated from the O-H bond in $Ca(OH)_2$, which reduced the pattern of the modified samples, indicating that $Ca(OH)_2$ was consumed by the SCMs in the pastes. The Si-O stretching vibration band at 975 $cm^{-1}$ represents the C-S-H gel with systematically changing frequency and intensity with the $CaO/SiO_2$ ratio in C-S-H.

### *3.5. Microstructure Characteristics*

#### 3.5.1. Pore Structure

Mercury intrusion porosimetry (MIP) is a widely used technique for assessing the porosity and distribution of pore sizes in cement-based materials. Figure 12 shows the influence of silica fume and fly ash on the pore structure evolution and pore size distribution of the blended cement pastes after 28 days of curing. The pore size distribution of each mixture ranged from 0 to 10 µm. The specific pore volume exhibited a slight variation with an increase in pore diameter (>100 nm); however, a significant increase in pore volume was observed in the range of pore diameters less than 100 nm, as shown in Figure 12a. The

higher cumulative pore volume with fly ash is due to the lower pozzolanic reaction; as the reaction activates, the total pore volume and pore size would reduce. The differential curve in Figure 12b shows an unimodal pore size distribution, with the largest pore volume located at 26.30 nm for all mixes. The probable pore diameter corresponding to the peak of each differential curve reflects the refinement of pores and the pore size distribution shifts toward smaller pore size ranges. According to Zeng et al. (2012) [68], the measured pore size distribution can be classified into four size ranges: gel micropores (<10 nm), mesopores (10–50 nm), middle capillary pores (50–100 nm), and large capillary pores (>100 nm). The volume ratio of mesopores was the highest, followed by middle capillary pores for all mixes. The inclusion of silica fume and fly ash in blended pastes densifies the microstructure by pore filling and the pozzolanic reaction, which reduces the harmful macrocapillary pores (>50 nm) that are detrimental to the strength and increases the mesopores, which are less harmful to the strength of concrete.

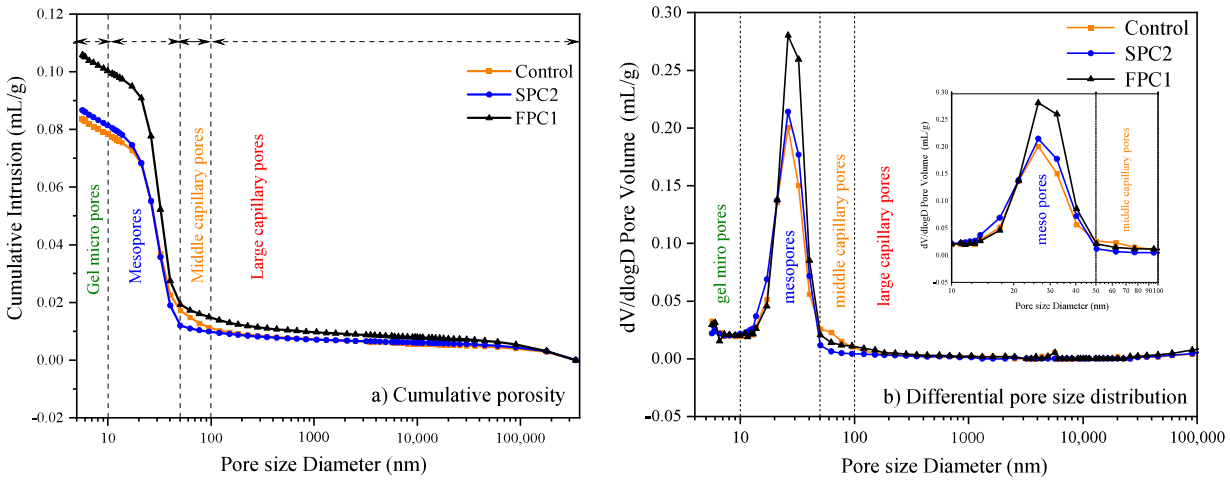


**Figure 12.** The porosity (**a**) and pore size distribution (**b**) of control and blended cement pastes at 28 days of standard curing.

### 3.5.2. Microstructure Morphology of Porous Concrete

SEM micrographs of fly ash, silica fume, and fiber-based pervious concrete after the compressive strength test are shown in Figures 13–15. A few partially reacted and broken fly ash particles with etched surfaces and hydrated rim encapsulation can be observed in Figure 13. The precipitation of $Ca(OH)_2$ and C-S-H on the etched surface of fly ash particles with an increase in the pozzolanic reaction reinforces the contact bonding between fly ash and cement, as well as fly ash particles, making the microstructure denser and more homogeneous and resulting in a remarkable long-term strength gain. The cracks detected in the SEM micrographs were assumed to be due to the compression strength test performed before the SEM investigation. In general, the elemental composition determined by EDS analysis indicates that Ca, O, Si, and Ai are the major elements comprising the C-S-H and C-A-S-H gels in the cementitious composite.

In PC5-PP-Rf, a few hydration particles and striations are visible on the fiber surface (Figure 15). In contrast, the PC2-FAP and PC4-SFP mixtures exhibited dense hydration products on the polypropylene fibers, leading to improved adhesion bonding between the interface matrix and the fibers. This enhanced the flexural strength of the reinforced porous concrete by increasing the bridging and pull-out resistance. The presence of fly ash and silica fume particles refines the pore enlargement caused by PPFs in the cement interface matrix through a micro-filling ability and pozzolanic reactions, which improves the mechanical properties of reinforced porous concrete. Proper amounts of PPFs combined with fly ash and silica fume ensured a uniform distribution throughout the matrix, enhancing the stress transformation between the interface matrix and fibers in the reinforced porous concrete.

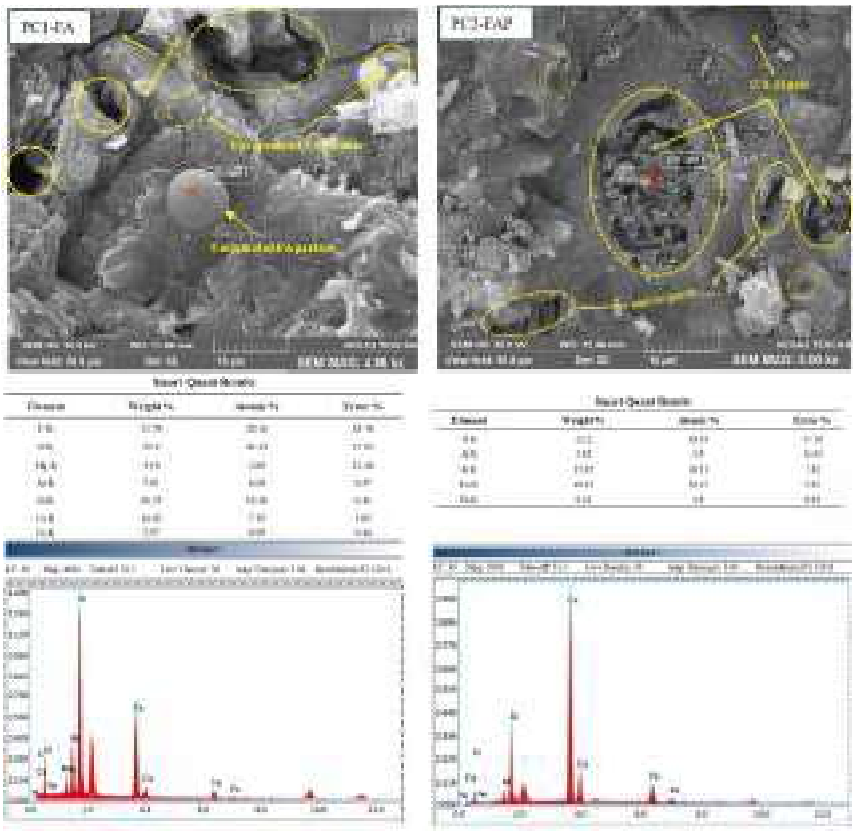


**Figure 13.** SEM and EDS micrographs of porous concrete after 28 days of standard curing: PC1-FA and PC2-FAP.

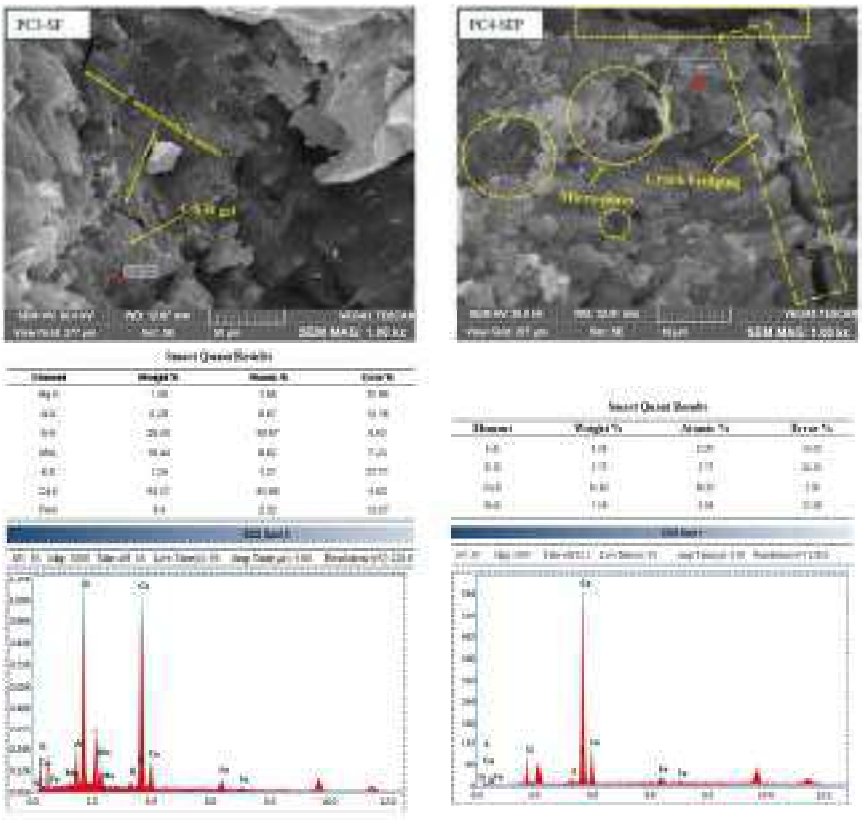


**Figure 14.** SEM and EDS micrographs of porous concrete after 28 days of standard curing: PC3-SF and PC4-SFP.

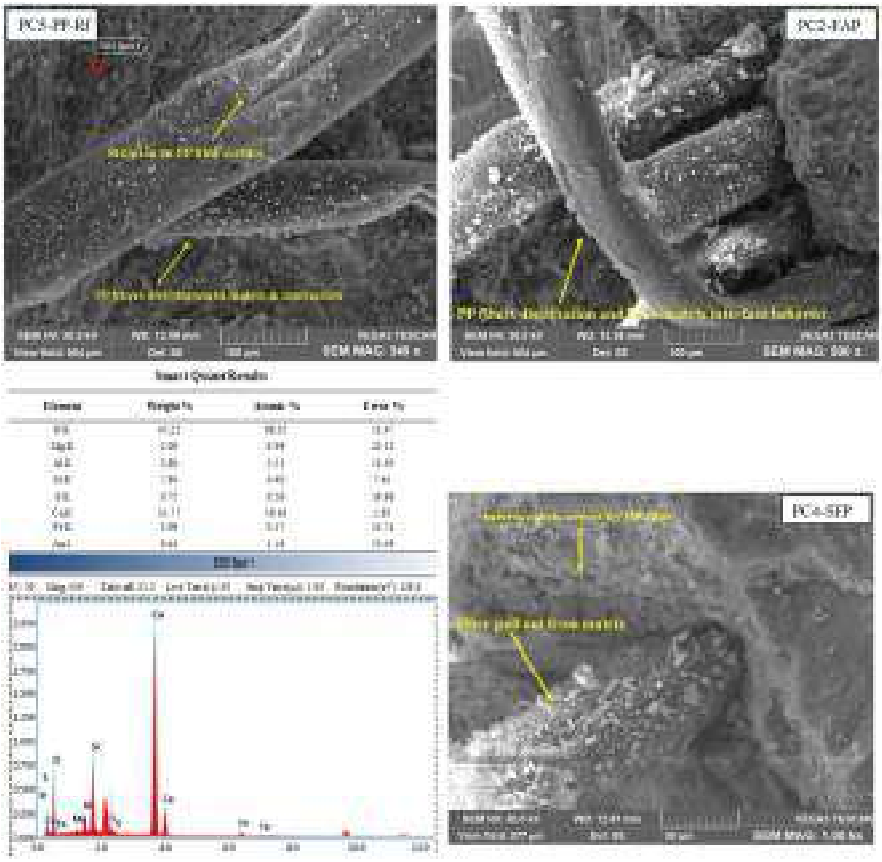


**Figure 15.** SEM and EDS micrographs of porous concrete after 28 days of standard curing: PC5-PP-Rf, PC2-FAP, and PC4SFP.

## 4. Conclusions

The following conclusions were derived by examining the impact of the B/A ratio, 5% fine sand, 10% fly ash or silica fume, and a binary combination of 10% fly ash or silica fume with 0.2% PPFs on the mechanical and durability characteristics of pervious concrete.

1. The binder-to-aggregate (B/A) ratio and compaction determine the strength and pore structure characteristics of the pervious concrete. The compressive strength increased with the B/A ratio up to an optimum limit of 0.28 and decreased beyond this limit. On the other hand, the increase in the B/A ratio always causes a reduction in porosity and permeability. Therefore, the choice of an appropriate B/A ratio requires the study of the variation in the skeleton pore structure. For the type of mix analyzed, the value of the B/A ratio being equal to 0.23 guarantees a good compromise that provides good compressive strength and optimal permeability.
2. Pervious concrete produced with fly ash or silica fume achieved the highest compressive strength (>35 MPa) at 28 days but had inferior flexural and tensile strengths compared to fiber-reinforced pervious concrete. The permeability was reduced by 10% fly ash or silica fume with 5% fine sand in pervious concrete; however, the binary combination of either fly ash or silica fume with polypropylene fibers enhanced the pore connectivity, thus yielding higher strength indices with adequate permeability greater than 5 mm/s.
3. Silica fume with fiber-reinforced pervious concrete exhibited the lowest mass loss based on abrasion and F-T durability performance criteria. Fiber-reinforced pervious concrete showed a similar mass loss to the silica fume fiber-reinforced based mix but improved the overall degradation resistance by reinforcing and bridging the aggregate and cementitious matrix together. Fly ash-based mixtures demonstrated

more significant mass loss due to the substantial uptake of water during consecutive F-T cycles.

4. Microstructural analysis showed that pervious concrete produced with an appropriate amount of PPFs and fly ash or silica fume led to a uniform distribution of fibers in the matrix, thus improving the stress transformation between the interface matrix and the fibers through bridging effects in the reinforced pervious concrete. The inclusion of fly ash or silica fume reduced the harmful capillary pores and refined the pore enlargement caused by PPFs in the cement interface matrix through micro-filling and a pozzolanic reaction, leading to improved mechanical properties and durability characteristics of pervious concrete.
5. The durability of reinforced pervious concrete, particularly in terms of its clogging resistance, is crucial for maintaining its long-term permeability. This aspect has not been investigated in this study; therefore, the conclusions and the results should be coupled with the clogging resistance characteristics to be obtained by further experimental studies.
6. The characteristics (mechanical and physical) of pervious concrete here proposed and investigated comply with the requirements of the specific standard codes for pervious concrete (e.g., the American ACI SPEC-522.1-13 [69] or the Chinese CJJ/T 135-2009 [70] and JC/T 2558-2020 [71]). Therefore, each mix is suitable for practical applications that are consistent with the objectives of the users.

**Author Contributions:** Conceptualization, X.G., L.C., H.B. and M.R.; methodology, X.G., H.B. and M.R.; software, H.B., L.C. and A.K.; validation, X.G., L.C., H.B., M.R. and AK.; formal analysis, H.B.; investigation, H.B. and M.R.; resources, X.G.; data curation, H.B.; writing—original draft preparation, H.B.; writing—review and editing, X.G., L.C. and M.R.; visualization, H.B., L.C. and A.K.; supervision, X.G. and L.C.; project administration, X.G. and M.R.; funding acquisition, X.G. All authors have read and agreed to the published version of the manuscript.

**Funding:** This research was funded by the Provincial Applied Technology Research and Development Major Project, grant number GA20C010 and the Natural Science Foundation of Heilongjiang Province of China, grant number LH2021E113.

**Data Availability Statement:** The original contributions presented in the study are included in the article; further inquiries can be directed to the corresponding author.

**Acknowledgments:** The authors would like to acknowledge the administrative and technical support provided by the School of Civil Engineering, Harbin Institute of Technology, China, particularly those research fellows in the Civil Engineering Materials Research Group, during the preparation and experimental testing.

**Conflicts of Interest:** The authors declare no conflicts of interest. The funders had no role in the design of the study; in the collection, analyses, or interpretation of data; in the writing of the manuscript; or in the decision to publish the results.

## Abbreviations

| | |
|---|---|
| B/A | Binder-to-aggregate ratio |
| A/B | Aggregate-to-binder ratio |
| W/C | Water-to-cement ratio |
| SP | Superplasticizer |
| PPFs | Polypropylene fibers |
| FHS | Frost-heaving stress |
| FA | Fly ash |
| SF | Silica fume |
| XRD | X-ray diffraction |
| FTIR | Fourier transform infrared spectroscopy |
| SEM | Scanning electron microscopy |
| EDS | Energy dispersive spectroscopy |

| | |
|---|---|
| XRF. | X-ray fluorescence spectrometry |
| TGA | Thermogravimetric analysis |
| DTA | Differential thermal analysis |
| SEM-EDS | Scanning electron microscopy equipped with energy dispersive spectroscopy |
| MIP | Mercury intrusion porosimetry |

## References


1. Sahdeo, S.K.; Ransinchung, G.D.; Rahul, K.L.; Debbarma, S. Effect of Mix Proportion on the Structural and Functional Properties of Pervious Concrete Paving Mixtures. *Constr. Build. Mater.* **2020**, *255*, 119260. [CrossRef]
2. Khankhaje, E.; Salim, M.R.; Mirza, J.; Salmiati; Hussin, M.W.; Khan, R.; Rafieizonooz, M. Properties of Quiet Pervious Concrete Containing Oil Palm Kernel Shell and Cockleshell. *Appl. Acoust.* **2017**, *122*, 113–120. [CrossRef]
3. Chu, L.; Fwa, T.F.; Tan, K.H. Laboratory Evaluation of Sound Absorption Characteristics of Pervious Concrete Pavement Materials. *Transp. Res. Rec. J. Transp. Res. Board* **2017**, *2629*, 91–103. [CrossRef]
4. Li, H.; Harvey, J.; Ge, Z. Experimental Investigation on Evaporation Rate for Enhancing Evaporative Cooling Effect of Permeable Pavement Materials. *Constr. Build. Mater.* **2014**, *65*, 367–375. [CrossRef]
5. Guan, X.; Wang, J.; Xiao, F. Sponge City Strategy and Application of Pavement Materials in Sponge City. *J. Clean. Prod.* **2021**, *303*, 127022. [CrossRef]
6. Li, H.; Ding, L.; Ren, M.; Li, C.; Wang, H. Sponge City Construction in China: A Survey of the Challenges and Opportunities. *Water* **2017**, *9*, 594. [CrossRef]
7. Wang, C.; Hou, J.; Miller, D.; Brown, I.; Jiang, Y. Flood Risk Management in Sponge Cities: The Role of Integrated Simulation and 3D Visualization. *Int. J. Disaster Risk Reduct.* **2019**, *39*, 101139. [CrossRef]
8. Ding, L.; Ren, X.; Gu, R.; Che, Y. Implementation of the "Sponge City" Development Plan in China: An Evaluation of Public Willingness to Pay for the Life-Cycle Maintenance of Its Facilities. *Cities* **2019**, *93*, 13–30. [CrossRef]
9. Hou, X.; Guo, H.; Wang, F.; Li, M.; Xue, X.; Liu, X.; Zeng, S. Is the Sponge City Construction Sufficiently Adaptable for the Future Stormwater Management under Climate Change? *J. Hydrol.* **2020**, *588*, 125055. [CrossRef]
10. Nguyen, T.T.; Ngo, H.H.; Guo, W.; Wang, X.C. A New Model Framework for Sponge City Implementation: Emerging Challenges and Future Developments. *J. Environ. Manage.* **2020**, *253*, 109689. [CrossRef]
11. Li, Q.; Wang, F.; Yu, Y.; Huang, Z.; Li, M.; Guan, Y. Comprehensive Performance Evaluation of LID Practices for the Sponge City Construction: A Case Study in Guangxi, China. *J. Environ. Manage.* **2019**, *231*, 10–20. [CrossRef] [PubMed]
12. López-Carrasquillo, V.; Hwang, S. Comparative Assessment of Pervious Concrete Mixtures Containing Fly Ash and Nanomaterials for Compressive Strength, Physical Durability, Permeability, Water Quality Performance and Production Cost. *Constr. Build. Mater.* **2017**, *139*, 148–158. [CrossRef]
13. Grubeša, I.N.; Barišić, I.; Ducman, V.; Korat, L. Draining Capability of Single-Sized Pervious Concrete. *Constr. Build. Mater.* **2018**, *169*, 252–260. [CrossRef]
14. Zhang, G.; Wang, S.; Wang, B.; Zhao, Y.; Kang, M.; Wang, P. Properties of Pervious Concrete with Steel Slag as Aggregates and Different Mineral Admixtures as Binders. *Constr. Build. Mater.* **2020**, *257*, 119543. [CrossRef]
15. Adil, G.; Kevern, J.T.; Mann, D. Influence of Silica Fume on Mechanical and Durability of Pervious Concrete. *Constr. Build. Mater.* **2020**, *247*, 118453. [CrossRef]
16. Giustozzi, F. Polymer-Modified Pervious Concrete for Durable and Sustainable Transportation Infrastructures. *Constr. Build. Mater.* **2016**, *111*, 502–512. [CrossRef]
17. Wu, H.; Liu, Z.; Sun, B.; Yin, J. Experimental Investigation on Freeze–Thaw Durability of Portland Cement Pervious Concrete (PCPC). *Constr. Build. Mater.* **2016**, *117*, 63–71. [CrossRef]
18. Yang, Z. Freezing-and-Thawing Durability of Pervious Concrete under Simulated Field Conditions. *Mater. J.* **2011**, *108*, 187–195.
19. Huang, B.; Wu, H.; Shu, X.; Burdette, E.G. Laboratory Evaluation of Permeability and Strength of Polymer-Modified Pervious Concrete. *Constr. Build. Mater.* **2010**, *24*, 818–823. [CrossRef]
20. Shu, X.; Huang, B.; Wu, H.; Dong, Q.; Burdette, E.G. Performance Comparison of Laboratory and Field Produced Pervious Concrete Mixtures. *Constr. Build. Mater.* **2011**, *25*, 3187–3192. [CrossRef]
21. Bilal, H.; Chen, T.; Ren, M.; Gao, X.; Su, A. Influence of Silica Fume, Metakaolin & SBR Latex on Strength and Durability Performance of Pervious Concrete. *Constr. Build. Mater.* **2021**, *275*, 122124. [CrossRef]
22. Nguyen, D.H.; Boutouil, M.; Sebaibi, N.; Baraud, F.; Leleyter, L. Durability of Pervious Concrete Using Crushed Seashells. *Constr. Build. Mater.* **2017**, *135*, 137–150. [CrossRef]
23. Ibrahim, H.A.; Abdul Razak, H.; Abutaha, F. Strength and Abrasion Resistance of Palm Oil Clinker Pervious Concrete under Different Curing Method. *Constr. Build. Mater.* **2017**, *147*, 576–587. [CrossRef]
24. Gesoğlu, M.; Güneyisi, E.; Khoshnaw, G.; İpek, S. Abrasion and Freezing–Thawing Resistance of Pervious Concretes Containing Waste Rubbers. *Constr. Build. Mater.* **2014**, *73*, 19–24. [CrossRef]
25. Gaedicke, C.; Marines, A.; Miankodila, F. Assessing the Abrasion Resistance of Cores in Virgin and Recycled Aggregate Pervious Concrete. *Constr. Build. Mater.* **2014**, *68*, 701–708. [CrossRef]

26. Toghroli, A.; Mehrabi, P.; Shariati, M.; Trung, N.T.; Jahandari, S.; Rasekh, H. Evaluating the Use of Recycled Concrete Aggregate and Pozzolanic Additives in Fiber-Reinforced Pervious Concrete with Industrial and Recycled Fibers. *Constr. Build. Mater.* **2020**, *252*, 118997. [CrossRef]
27. Dai, Z.; Li, H.; Zhao, W.; Wang, X.; Wang, H.; Zhou, H.; Yang, B. Multi-Modified Effects of Varying Admixtures on the Mechanical Properties of Pervious Concrete Based on Optimum Design of Gradation and Cement-Aggregate Ratio. *Constr. Build. Mater.* **2020**, *233*, 117178. [CrossRef]
28. Lian, C.; Zhuge, Y. Optimum Mix Design of Enhanced Permeable Concrete—An Experimental Investigation. *Constr. Build. Mater.* **2010**, *24*, 2664–2671. [CrossRef]
29. Zhong, R.; Wille, K. Compression Response of Normal and High Strength Pervious Concrete. *Constr. Build. Mater.* **2016**, *109*, 177–187. [CrossRef]
30. Lang, L.; Duan, H.; Chen, B. Properties of Pervious Concrete Made from Steel Slag and Magnesium Phosphate Cement. *Constr. Build. Mater.* **2019**, *209*, 95–104. [CrossRef]
31. Yang, J.; Jiang, G. Experimental Study on Properties of Pervious Concrete Pavement Materials. *Cem. Concr. Res.* **2003**, *33*, 381–386. [CrossRef]
32. Kevern, J.T.; Biddle, D.; Cao, Q. Effects of Macrosynthetic Fibers on Pervious Concrete Properties. *J. Mater. Civ. Eng.* **2015**, *27*, 06014031. [CrossRef]
33. Huang, J.; Luo, Z.; Khan, M.B.E. Impact of Aggregate Type and Size and Mineral Admixtures on the Properties of Pervious Concrete: An Experimental Investigation. *Constr. Build. Mater.* **2020**, *265*, 120759. [CrossRef]
34. Saboo, N.; Shivhare, S.; Kori, K.K.; Chandrappa, A.K. Effect of Fly Ash and Metakaolin on Pervious Concrete Properties. *Constr. Build. Mater.* **2019**, *223*, 322–328. [CrossRef]
35. Wang, H.; Li, H.; Liang, X.; Zhou, H.; Xie, N.; Dai, Z. Investigation on the Mechanical Properties and Environmental Impacts of Pervious Concrete Containing Fly Ash Based on the Cement-Aggregate Ratio. *Constr. Build. Mater.* **2019**, *202*, 387–395. [CrossRef]
36. Nazeer, M.; Kapoor, K.; Singh, S.P. Strength, Durability and Microstructural Investigations on Pervious Concrete Made with Fly Ash and Silica Fume as Supplementary Cementitious Materials. *J. Build. Eng.* **2023**, *69*, 106275. [CrossRef]
37. Kevern, J.; Wang, K.; Suleiman, M.T.; Schaefer, V.R. Mix Design Development for Pervious Concrete in Cold Weather Cli-Mates. In Proceedings of the 2005 Mid-Continent Transportation Research Symposium, Ames, IA, USA, 18–19 August 2005; Iowa State University: Ames, IA, USA, 2005. Available online: https://rosap.ntl.bts.gov/view/dot/38663/dot_38663_ds1.pdf (accessed on 1 October 2024).
38. Kevern, J.T.; Schaefer, V.R.; Wang, K.; Suleiman, M.T. Pervious Concrete Mixture Proportions for Improved Freeze-Thaw Durability. *J. ASTM Int.* **2008**, *5*, 1–12. [CrossRef]
39. Wu, H.; Huang, B.; Shu, X.; Dong, Q. Laboratory Evaluation of Abrasion Resistance of Portland Cement Pervious Concrete. *J. Mater. Civ. Eng.* **2011**, *23*, 697–702. [CrossRef]
40. Bright Singh, S.; Murugan, M. Effect of Aggregate Size on Properties of Polypropylene and Glass Fibre-Reinforced Pervious Concrete. *Int. J. Pavement Eng.* **2022**, *23*, 2034–2048. [CrossRef]
41. Juradin, S.; Netinger-Grubeša, I.; Mrakovčić, S.; Jozić, D. Impact of Fibre Incorporation and Compaction Method on Properties of Pervious Concrete. *Mater. Constr.* **2021**, *71*, e245. [CrossRef]
42. Furkan Ozel, B.; Sakallı, Ş.; Şahin, Y. The Effects of Aggregate and Fiber Characteristics on the Properties of Pervious Concrete. *Constr. Build. Mater.* **2022**, *356*, 129294. [CrossRef]
43. Akand, L.; Yang, M.; Wang, X. Effectiveness of Chemical Treatment on Polypropylene Fibers as Reinforcement in Pervious Concrete. *Constr. Build. Mater.* **2018**, *163*, 32–39. [CrossRef]
44. Wu, J.; Hu, L.; Hu, C.; Wang, Y.; Zhou, J.; Li, X. Impact of Polypropylene Fiber on the Mechanical and Physical Properties of Pervious Concrete: An Experimental Investigation. *Buildings* **2023**, *13*, 1966. [CrossRef]
45. Qin, L.; Gao, X.; Chen, T. Influence of Mineral Admixtures on Carbonation Curing of Cement Paste. *Constr. Build. Mater.* **2019**, *212*, 653–662. [CrossRef]
46. *GT/B 50081–2002*; Standard for Test Method of Mechanical Properties in Ordinary Concrete. Ministry of Housing and Urban-Rural Development of China (MOHURD): Beijing, China, 2002.
47. *GT/B 50082-2009*; Revised Standard for Test Methods of Long-Term Performance and Durability of Ordinary Concrete. Ministry of Housing and Urban-Rural Development of China (MOHURD): Beijing, China, 2009.
48. Khankhaje, E.; Kim, T.; Jang, H.; Kim, C.-S.; Kim, J.; Rafieizonooz, M. Properties of Pervious Concrete Incorporating Fly Ash as Partial Replacement of Cement: A Review. *Dev. Built Environ.* **2023**, *14*, 100130. [CrossRef]
49. Jiang, Z.W.; Sun, Z.P.; Wang, P.M. Effects of Some Factors on Properties of Porous Pervious Concrete. *J. Build. Mater.* **2005**, *8*, 513–519.
50. Zhang, C.; Zhang, X.; Hou, J.; Wang, J.; Duan, G. Rheology and Early Microstructure Evolution of Fresh Ultra-High Performance Concrete with Polycarboxylate Superplasticizer. *Case Stud. Constr. Mater.* **2022**, *17*, e01575. [CrossRef]
51. Xiong, B.; Gao, H.; Lu, X.; Tian, B.; Zhang, P.; Chen, B. Influence of Maximum Paste Coating Thickness without Void Clogging on the Pore Characteristics and Seepage Flow of Pervious Concrete. *Constr. Build. Mater.* **2023**, *392*, 131979. [CrossRef]
52. Pereira Da Costa, F.B.; Haselbach, L.M.; Da Silva Filho, L.C.P. Pervious Concrete for Desired Porosity: Influence of w/c Ratio and a Rheology-Modifying Admixture. *Constr. Build. Mater.* **2021**, *268*, 121084. [CrossRef]

53. Luo, Y.; Lv, Y.; Wang, D.; Jiang, Z.; Xue, G. The Influence of Coarse Aggregate Gradation on the Mechanical Properties, Durability, and Plantability of Geopolymer Pervious Concrete. *Constr. Build. Mater.* **2023**, *382*, 131246. [CrossRef]
54. Claudino, G.O.; Rodrigues, G.G.O.; Rohden, A.B.; Mesquita, E.F.T.; Garcez, M.R. Mix Design for Pervious Concrete Based on the Optimization of Cement Paste and Granular Skeleton to Balance Mechanical Strength and Permeability. *Constr. Build. Mater.* **2022**, *347*, 128620. [CrossRef]
55. Yogesh, R.V.; Santha, G.K.; Ganesh, K.S. Synergistic Effect of Aggregate Gradation Band and Cement to Aggregate Ratio on the Performance of Pervious Concrete. *J. Build. Eng.* **2023**, *73*, 106718. [CrossRef]
56. Xie, X.; Zhang, T.; Wang, C.; Yang, Y.; Bogush, A.; Khayrulina, E.; Huang, Z.; Wei, J.; Yu, Q. Mixture Proportion Design of Pervious Concrete Based on the Relationships between Fundamental Properties and Skeleton Structures. *Cem. Concr. Compos.* **2020**, *113*, 103693. [CrossRef]
57. Neithalath, N.; Sumanasooriya, M.S.; Deo, O. Characterizing Pore Volume, Sizes, and Connectivity in Pervious Concretes for Permeability Prediction. *Mater. Charact.* **2010**, *61*, 802–813. [CrossRef]
58. Li, H.; Yang, J.; Yu, X.; Zhang, Y.; Zhang, L. Permeability Prediction of Pervious Concrete Based on Mix Proportions and Pore Characteristics. *Constr. Build. Mater.* **2023**, *395*, 132247. [CrossRef]
59. Chen, X.; Wang, H.; Najm, H.; Venkiteela, G.; Hencken, J. Evaluating Engineering Properties and Environmental Impact of Pervious Concrete with Fly Ash and Slag. *J. Clean. Prod.* **2019**, *237*, 117714. [CrossRef]
60. Kia, A. Freeze-Thaw Durability of Air-Entrained High-Strength Clogging Resistant Permeable Pavements. *Constr. Build. Mater.* **2023**, *400*, 132767. [CrossRef]
61. Mohammed, B.S.; Liew, M.S.; Alaloul, W.S.; Khed, V.C.; Hoong, C.Y.; Adamu, M. Properties of Nano-Silica Modified Pervious Concrete. *Case Stud. Constr. Mater.* **2018**, *8*, 409–422. [CrossRef]
62. Chen, Y.; Wang, K.; Wang, X.; Zhou, W. Strength, Fracture and Fatigue of Pervious Concrete. *Constr. Build. Mater.* **2013**, *42*, 97–104. [CrossRef]
63. Nili, M.; Afroughsabet, V. The Long-Term Compressive Strength and Durability Properties of Silica Fume Fiber-Reinforced Concrete. *Mater. Sci. Eng. A* **2012**, *531*, 107–111. [CrossRef]
64. Zhong, R.; Wille, K. Influence of Matrix and Pore System Characteristics on the Durability of Pervious Concrete. *Constr. Build. Mater.* **2018**, *162*, 132–141. [CrossRef]
65. Monteagudo, S.M.; Moragues, A.; Gálvez, J.C.; Casati, M.J.; Reyes, E. The Degree of Hydration Assessment of Blended Cement Pastes by Differential Thermal and Thermogravimetric Analysis. Morphological Evolution of the Solid Phases. *Thermochim. Acta* **2014**, *592*, 37–51. [CrossRef]
66. Bhattacharya, M.; Harish, K.V. An Integrated Approach for Studying the Hydration of Portland Cement Systems Containing Silica Fume. *Constr. Build. Mater.* **2018**, *188*, 1179–1192. [CrossRef]
67. Hanehara, S.; Tomosawa, F.; Kobayakawa, M.; Hwang, K. Effects of Water/Powder Ratio, Mixing Ratio of Fly Ash, and Curing Temperature on Pozzolanic Reaction of Fly Ash in Cement Paste. *Cem. Concr. Res.* **2001**, *31*, 31–39. [CrossRef]
68. Zeng, Q.; Li, K.; Fen-chong, T.; Dangla, P. Pore Structure Characterization of Cement Pastes Blended with High-Volume Fly-Ash. *Cem. Concr. Res.* **2012**, *42*, 194–204. [CrossRef]
69. *ACI Committee 522; ACI SPEC-522.1-13*; Specification for Pervious Concrete Pavement. American Concrete Institute: Hills, MI, USA, 2013.
70. *CJJ/T 135-2009*; Technical Specification for Pervious Cement Concrete Pavement. Standards Press of China: Beijing, China, 2023.
71. *JC/T 2558-2020*; Pervious Concrete. Standards Press of China: Beijing, China, 2020.